Volume 55 | Number 63 | 14 August 2019 | Pages 9219–9404

ChemComm

Chemical Communications

rsc.li/chemcomm

ISSN 1359-7345

ROYAL SOCIETY OF CHEMISTRY | Celebrating IYPT 2019

COMMUNICATION

Antonio Rodríguez-Fortea, Ning Chen *et al.*

Th@C_1(11)-C_{86}: an actinide encapsulated in an unexpected C_{86} fullerene cage

ChemComm

COMMUNICATION

Cite this: *Chem. Commun.*, 2019, **55**, 9271

Received 17th June 2019,
Accepted 4th July 2019

DOI: 10.1039/c9cc04613e

rsc.li/chemcomm

Th@C_1(11)-C_{86}: an actinide encapsulated in an unexpected C_{86} fullerene cage†

Yaofeng Wang,‡[a] Roser Morales-Martínez,‡[b] Wenting Cai,‡[c] Jiaxin Zhuang,[a] Wei Yang,[a] Luis Echegoyen,[c] Josep M. Poblet,[b] Antonio Rodríguez-Fortea*[b] and Ning Chen*[a]

A novel actinide endohedral fullerene with an unexpected chiral cage, Th@C_1(11)-C_{86}, was synthesized and characterized. DFT calculations suggest that this low symmetry cage was favoured as a consequence of the strong interaction between Th and the cage, which makes the predictions by the ionic model less reliable for these endohedral mono-metallofullerenes.

Endohedral metallofullerenes (EMFs) have aroused widespread concern due to their fascinating properties and broad applications in materials science, photovoltaics, electronics, and biomedicine.[1–3] The earliest studied EMFs are endohedral mono-metallofullerenes (mono-EMFs) which started with the discovery of La@C_{60}^+ in the gas phase by Smalley *et al.* in 1985.[4] Since then, mono-EMFs have undergone a dramatic development over the last 30 years, and mono-EMFs with a broad range of carbon cages and metal elements have been successfully synthesized. Up to now, the reported mono-EMFs have been centred on group 2 and 3 metallofullerenes such as Sc,[5] Y,[6] La,[7] Ca[8] and Ba[9] as well as lanthanide metallofullerenes (Ce–Lu).[10–17] Very recently, we successfully synthesized and characterized a series of actinide EMFs based on uranium and thorium.[18–20] Among them, Th@C_{3v}(8)-C_{82} is the first isolated metallofullerene with unique four electron transfer from metal to the carbon cage.[19] U@C_{2n} ($2n$ = 74, 82) show surprising metal oxidation state dependence on carbon cage isomerism.[18] Our very recent discovery of three novel non-IPR actinide mono-EMFs, U@C_1(17 418)-C_{76}, U@C_1(28 324)-C_{80}, and Th@C_1(28 324)-C_{80}, revealed that actinides tend to select low symmetry cages which do not obey the isolated pentagon rule, due to the significantly strong host–guest interactions between the actinide ions and the fullerene cages.[20] All these results demonstrate that the monoactinide EMFs have remarkably different structural and electronic properties from those previously investigated lanthanide EMFs. A continuous effort would be, then, essential to get further insight into this novel fullerene family.

Here, we report that the unique four electron transfer from Th metal to the fullerene cage stabilized a chiral C_1(11)-C_{86} fullerene cage, which has never been discovered before, either in empty fullerenes or EMFs. This novel actinide EMF was fully characterized by single-crystal X-ray diffraction, various spectroscopies, electrochemistry and DFT calculations.

Th@C_{86} was synthesized in a modified arc-discharge reactor with a ThO_2/graphite powder mixture (molar ratio of Th/C = 1 : 24) under a 200 Torr helium atmosphere. The resulting soot was refluxed in chlorobenzene under an argon atmosphere for 12 h. Multistage HPLC separation procedures gave a pure isomer of Th@C_{86} (see Fig. S1, ESI†). The purified sample was confirmed by the final chromatogram and positive-ion mode matrix-assisted laser desorption/ionization-time of flight mass spectrometry (MALDI-TOF MS) spectrum shown in Fig. 1. The isotopic distribution of the experimental spectrum agrees well with the theoretical calculation for Th@C_{86}, as seen in the inset.

Single crystals of Th@C_{86} were obtained by layering a benzene solution of Ni^{II}(OEP) (OEP = 2,3,7,8,12,13,17,18-octaethylporphyrin dianion) over a nearly saturated solution of Th@C_{86} in CS_2 in a glass tube. The molecular structure of Th@C_{86} was unambiguously determined in a monoclinic $C2/m$ (No. 12) space group by single-crystal X-ray diffraction. Interestingly, the crystallographic data indicate that Th@C_{86} utilizes a carbon cage with C_1 symmetry, namely the C_1(11)-C_{86} cage, which is the eleventh isomer of C_{86} that obeys the isolated pentagon rule according to the spiral algorithm.[21]

Fig. 2 shows the X-ray structure of Th@C_1(11)-C_{86} together with a cocrystallized [Ni^{II}(OEP)] moiety. As expected, a host–guest interaction was observed between the fullerene cage and the Ni^{II}(OEP) moiety with a shortest Ni-to-cage carbon distance (Ni1–C9C) of 2.928 Å, indicating a typical π–π stacking

[a] *Laboratory of Advanced Optoelectronic Materials, College of Chemistry, Chemical Engineering and Materials Science, Soochow University, Suzhou, Jiangsu, 215123, P. R. China. E-mail: chenning@suda.edu.cn*

[b] *Departament de Química Física i Inorgànica, Universitat Rovira i Virgili, c/Marcel·lí Domingo 1, 43007 Tarragona, Spain. E-mail: antonio.rodriguezf@urv.cat*

[c] *Department of Chemistry, University of Texas at El Paso, 500 W University Avenue, El Paso, Texas 79968, USA*

† Electronic supplementary information (ESI) available. CCDC 1829174. For ESI and crystallographic data in CIF or other electronic format see DOI: 10.1039/c9cc04613e

‡ These authors contributed equally to this work.

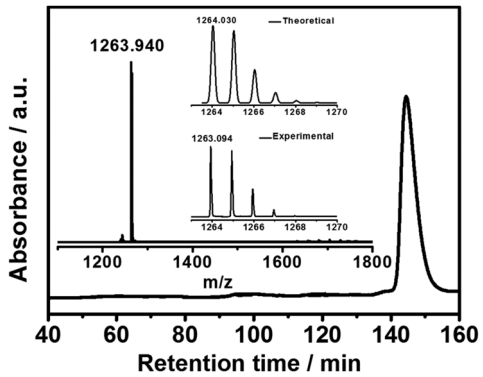

Fig. 1 HPLC chromatogram of purified Th@C_{86} on a Buckyprep column with toluene as the eluent (HPLC condition: flow rate: 4 mL min^{-1}. The inset shows the positive-ion mode MALDI-TOF mass spectrum and expansion of the observed isotopic distribution of Th@C_{86} in comparison with the calculated one).

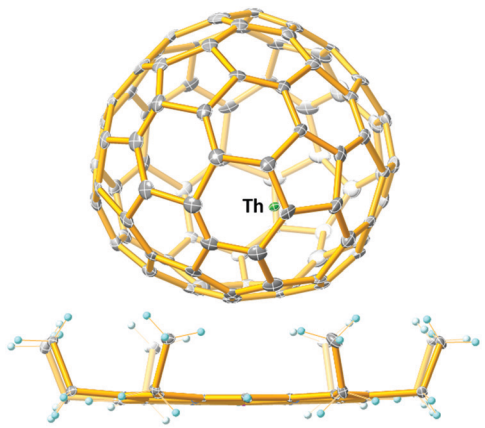

Fig. 2 ORTEP drawing of Th@C_1(11)-C_{86}·[Ni^{II}(OEP)] with 25% thermal ellipsoids, showing the relationship between the fullerene cage and [Ni^{II}(OEP)]. Only the major thorium site (Th1 with 0.31 occupancy) is shown. The solvent molecules and minor metal sites are omitted for clarity.

interaction between the fullerene and porphyrin moieties. For Th@C_1(11)-C_{86}, a mirror-related cage is generated by crystallographic operation due to the high symmetric $C2/m$ space group. As shown in Fig. S2 (ESI†), it is obvious that these two C_1(11)-C_{86} cages (cage 1 and cage 1A) are enantiomeric species, possessing a $^{f,s}C$ configuration and a $^{f,s}A$ configuration, respectively. The stereodescriptors $^{f,s}C$ and $^{f,s}A$ (f = fullerene; s = systematic numbering) depend on whether the contiguous numbering of the cage is clockwise or anticlockwise. Accordingly, the obtained cocrystal contains racemic Th@C_1(11)-C_{86} with two enantiomers each having occupancy values of 0.5, respectively.

Interestingly, though C_{86} could have as many as 19 IPR cage isomers, only three of them were reported and crystallographically confirmed. Among them, all of the C_{86}-based nitride clusterfullerenes (NCFs) are found to adopt a D_3(19)-C_{86} cage, such as $Dy_xSc_{3-x}N@D_3$(19)-C_{86},[22] $Gd_3N@D_3$(19)-C_{86},[23] $Tb_3N@D_3$(19)-C_{86},[24] and $Lu_3N@D_3$(19)-C_{86}.[25] In addition, Echegoyen *et al.* found Sc_2C_2@C_{2v}(9)-C_{86} with a planar, twisted Sc_2C_2 unit inside a C_{2v}(9)-C_{86} fullerene cage.[26] Lu *et al.* also reported a dimetallic EMF, $Lu_2@C_{2v}$(9)-C_{86}.[27] The discovery of Th@C_1(11)-C_{86} suggests that this novel chiral fullerene cage can be stabilized by the encapsulation of actinide metal ions.

Inside the cage, the Th atom shows some degree of disorder that only three Th ion positions have been assigned, with fractional occupancies of 0.02, 0.17 and 0.31 (see Fig. S3a and Table S1, ESI†). Interestingly, a similar phenomenon has been reported previously for the first crystallographic structure of thorium EMF Th@C_{3v}(8)-C_{82}.

It seems that the movement of the Th atom is severely hindered inside these fullerene cages, as compared to the largely free lanthanide metals inside the previously reported mono-metallofullerenes, an indication of the stronger interaction between the actinides and fullerene cages.

As shown in Fig. S3b (ESI†), the primary Th atom (Th1 with a fractional occupancy of 0.31) is located over a [5,6]-bond (*i.e.*, C65C and C81C) with the shortest Th–C distance in the range of 1.921–2.008 Å. Th1A (the mirror-related site of Th1) is generated by crystallographic operation shown in Fig. S3c (ESI†). It is situated over the center of a hexagon (C45C, C46C, C30C, C43C, C44C, and C45C) with the shortest Th–C distance in the range of 2.326–2.457 Å. Crystallographically, it is difficult to determine whether either or both of these two locations are occupied. Thus, computational studies are needed to further determine the optimized molecular structure of Th@C_1(11)-C_{86}.

In order to get a deeper understanding of the Th–cage interaction, DFT calculations at the BP86-DG3/TZP level (see the ESI† for more details) were performed to obtain the most stable locations of the metal inside the fullerene. We have already reported that the transfer of four electrons to the carbon cage induces strong interactions between the metal and the neighbouring carbons, and that the interaction energy can vary from one side to another in more than 40 kcal mol^{-1}.[20] As a consequence of these strong interactions, the predictions made by the ionic model are not as valid as for clusterfullerenes or mono-metallofullerenes with charge transfers smaller than four (see Table S3, ESI†). For the present cage, we have obtained a quite similar behaviour, as shown in Fig. 3. Among the different locations, the strongest stabilisations occur when Th interacts with the sumanene units present in IPR isomer 11 (there are two of them, see Fig. 3). These two positions for Th differ in 6 kcal mol^{-1}; when the metal is placed in other sites, the energy increases in a range between 23 and 39 kcal mol^{-1}. Recent computational studies already emphasized the affinity of Th for these sumanene motifs.[28] The difference between these two preferential locations of Th can be easily explained by means of molecular orbital interactions. As shown in Fig. S5 (ESI†), the LUMO+1 of the empty cage is mainly located in one of the sumanenes, consequently this orbital is more stabilised after the encapsulation of the Th in this site. However, the encapsulation of the Th near the other sumanene involves partially the LUMO+2 of the cage, thus, the corresponding molecular orbital is higher in energy. No significant stabilizations of the two cage orbitals that accept the four electrons from Th take place for those locations of Th at much higher energies (see Fig. S6, ESI†).

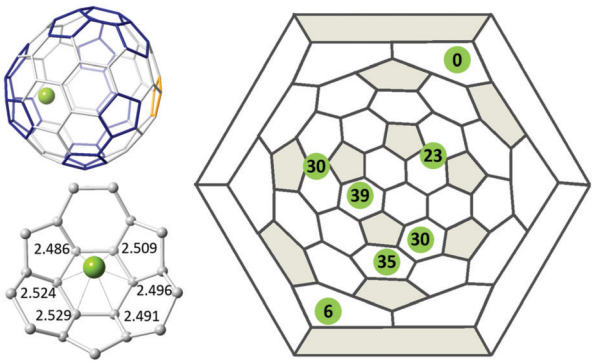

Fig. 3 Computed structure for Th@C_1(11)-C_{86} including the shortest Th–C distances (left), and Schlegel representation for C_1(11)-C_{86} where values represent different computed locations of Th inside the fullerene and their relative energies (in kcal mol^{-1}).

It is worth mentioning that the Th location with the lowest energy corresponds to the Th1A site in the crystallographic structure (Fig. 3). The computed Th–C distances fall in the range of 2.49–2.53 Å. These values follow the usual observation that DFT distances are always somewhat longer than the crystallographic ones. Given that all the shortest DFT distances for the seven computed locations fall in a similar range of 2.42–2.61 Å, we have to conclude that the crystallographic Th1–C distances (1.921–2.008 Å) are too short to correspond to real Th–fullerene contacts. Furthermore, to verify that C_1(11)-C_{86} is the most abundant isomer encapsulating a Th ion, we have selected the lowest in energy IPR isomers as tetraanions to check the relative stabilities for endohedral Th@C_{86}. Although C_{2v}(9)-C_{86} is the most stable isomer in the ionic form, the C_1(11)-C_{86} cage is much more stabilised after the actinide encapsulation, becoming the most stable one followed by C_s(15)-C_{86} and C_2(14)-C_{86}, both EMFs with relative energies below 3.5 kcal mol^{-1} (Table S3, ESI†). We have recently seen that mono-metallofullerenes with formal charge transfers of four electrons hardly follow the ionic model, in contrast to clusterfullerenes.[20] Computed abundances show that Th@C_1(11)-C_{86} is the most favourable EMF in the whole range of temperatures (Fig. S7, ESI†).

The purified sample of Th@C_1(11)-C_{86} dissolved in CS_2 was characterized by UV-vis-NIR absorption spectroscopy. The absorption spectra of endohedral fullerenes are typically attributed to the formal charge state and carbon cage symmetry.[29] As shown in Fig. 4, the spectral onset of Th@C_1(11)-C_{86} is located at around 1287 nm, which results in an optical band gap of 0.96 V. Moreover, Th@C_{86} displays minor absorption bands at 474 nm, and two distinct absorptions at 630 and 1190 nm. These absorption features are substantially different from those of the previously reported compounds involving the C_{86} cage, which are consistent with the presence of a different carbon cage symmetry in the present cage.[27,30,31]

Fig. 5 presents the low energy Raman spectrum of Th@C_1(11)-C_{86}. The low energy Raman spectra are sensitive to the metal–cage charge transfer and hence can afford a wealth of useful information on the metal–cage interaction and electronic structure of endohedral fullerenes. It is noteworthy that a sharp peak at

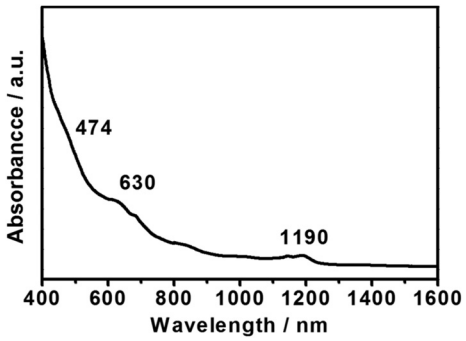

Fig. 4 UV-vis-NIR absorption spectrum of purified Th@C_{86} in CS_2.

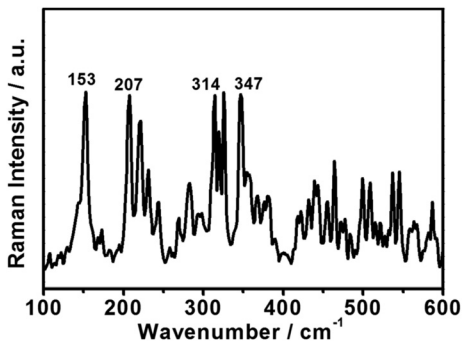

Fig. 5 Low energy Raman spectrum of Th@C_{86}.

153 cm^{-1} was observed and can be assigned to the metal-to-cage vibrational mode. This frequency of Th@C_1(11)-C_{86} (153 cm^{-1}) is very close to 148 cm^{-1} for Th@C_{3v}(8)-C_{82}[19] and 155 cm^{-1} for Th@C_1(28 324)-C_{80},[20] respectively, indicating similar metal-to-cage interaction in thorium-based endohedral mono-metallofullerenes. In addition, the frequencies of the cage vibration mode were found at 207, 314 and 347 cm^{-1} in the range of 200–500 cm^{-1}. These features show substantial differences compared to reported Gd_3N@C_{86},[32] indicating the differences between the two C_{86} cage isomers.

The redox properties of Th@C_1(11)-C_{86} were investigated by means of cyclic voltammetry (CV). The cyclic voltammogram of Th@C_1(11)-C_{86} shows three reversible and one irreversible processes along with one reversible oxidation and one irreversible oxidation process (Fig. S4, ESI†). This behaviour is different to other C_{86}-cage based fullerenes, such as M_3N@C_{86} (M = Gd, Nd, and Pr),[23,31] Sc_2C_2@C_{2v}(9)-C_{86},[26] Lu_2@C_{2v}(9)-C_{86},[27] and Sm@C_{86}.[33] Thus, changing the symmetry of the cage and the encapsulated cluster significantly affects the redox properties of endohedral fullerenes. The first oxidation and reduction potentials of Th@C_1(11)-C_{86} are 0.21 and −1.17 V, respectively, giving rise to a larger electrochemical gap of 1.38 V. This result correlates well with the optical band gap calculated by UV-vis-NIR absorption. Moreover, the EC band gap of Th@C_1(11)-C_{86} (1.38 V) is close to those of Lu_2@C_{2v}(9)-C_{86}, Sc_2C_2@C_{2v}(9)-C_{86}, Th@C_1(28 324)-C_{80} and Th@C_{3v}(8)-C_{82}, which transfer four electrons from atoms or clusters to the fullerene cages, as shown in Table 1. This confirms that Th@C_1(11)-C_{86} possesses the closed-shell electronic

Table 1 Redox potentials (V *vs.* Fc/Fc^+) and electrochemical band gaps of Th@C_1(11)-C_{86} and reference EMFs

Compound	$E^{+/0}$	$E^{0/-}$	$E^{-/2-}$	$E^{2-/3-}$	$E^{3-/4-}$	$E_{gap,ec}$ (V)	Ref.
Th@C_1(11)-C_{86}	+0.21[a]	−1.17[a]	−1.51[a]	−1.85[a]	−2.24[b]	1.38	This work
Th@C_{3v}(8)-C_{82}	+0.46[a]	−1.05[b]	−1.54[b]	−1.69[b]	−1.82[b]	1.51	19
Th@C_1(28 324)-C_{80}	+0.24[a]	−1.22[b]	−1.50[a]	−2.05[a]	−2.14[b]	1.46	20
Sm@C_{86}		−0.47[b]	−0.78[b]	−1.31[b]	−1.71[b]		33
Lu_2@C_{2v}(9)-C_{86}	0.31[a]	−1.01[b]	−1.34[b]			1.32	27
Sc_2C_2@C_{2v}(9)-C_{86}	+0.47[a]	−0.84[a]	−1.11[b]	−1.63[b]	−2.54[b]	1.31	26
Pr_3N@D_3(19)-C_{86}	+0.31[b]	−1.48[b]				1.79	31

[a] Half-wave potential (reversible redox process). [b] Peak potential (irreversible redox process).

structure and is consistent with the four-electron metal-cage charge transfer.

In summary, a novel actinide endohedral fullerene, Th@C_{86}, has been successfully synthesized and fully characterized by mass spectrometry, single-crystal X-ray crystallography, UV-vis-NIR spectroscopy, Raman spectroscopy, cyclic voltammetry and DFT calculations. Crystallographic analysis unambiguously assigned the molecular structure to Th@C_1(11)-C_{86}, which is predicted to be the most abundant cage for the whole range of temperatures according to thermodynamics. In addition, electrochemical investigations, as well as electronic structure calculations, demonstrated that Th@C_1(11)-C_{86} has a closed-shell electronic structure and four-electron metal-cage charge transfer with a strong Th–cage interaction that makes the predictions of the ionic model no longer valid. This work further highlights the evidence that actinide EMFs have remarkably different structural and electronic properties from previously investigated lanthanide EMFs, which deepens the understanding of unique actinide behaviours inside the fullerene cage.

C. N. thanks the National Science Foundation China (NSFC 51302178) and Priority Academic Program Development of Jiangsu Higher Education Institutions (PAPD). A. R.-F. and J. M. P. thank the Spanish Ministry of Science (CTQ2017-87269-P) for support. J. M. P. also thanks ICREA foundation for an ICREA ACADEMIA award. R. M. M. thanks the Spanish Ministry of Science for a PhD fellowship.

Conflicts of interest

There are no conflicts to declare.

Notes and references

1 W. Krätschmer, L. D. Lamb, K. Fostiropoulos and D. R. Huffman, *Nature*, 1990, **347**, 354.
2 S. Yang, T. Wei and F. Jin, *Chem. Soc. Rev.*, 2017, **46**, 5005–5058.
3 L. Bao, M. Chen, C. Pan, T. Yamaguchi, T. Kato, M. M. Olmstead, A. L. Balch, T. Akasaka and X. Lu, *Angew. Chem.*, 2016, **55**, 4242–4246.
4 J. R. Heath, S. C. O'Brien, Q. Zhang, Y. Liu, R. F. Curl, F. K. Tittel and R. E. Smalley, *J. Am. Chem. Soc.*, 1985, **107**, 7779–7780.
5 M. Hachiya, H. Nikawa, N. Mizorogi, T. Tsuchiya, X. Lu and T. Akasaka, *J. Am. Chem. Soc.*, 2012, **134**, 15550–15555.
6 L. Bao, C. Pan, Z. Slanina, F. Uhlik, T. Akasaka and X. Lu, *Angew. Chem., Int. Ed.*, 2016, **55**, 9234–9238.
7 T. Akasaka, X. Lu, H. Kuga, H. Nikawa, N. Mizorogi, Z. Slanina, T. Tsuchiya, K. Yoza and S. Nagase, *Angew. Chem.*, 2010, **49**, 9715–9719.
8 Z. Xu, T. Nakane and H. Shinohara, *J. Am. Chem. Soc.*, 1996, **118**, 11309–11310.
9 A. Reich, M. Panthöfer, H. Modrow, U. Wedig and M. Jansen, *J. Am. Chem. Soc.*, 2004, **126**, 14428–14434.
10 M. Suzuki, M. Yamada, Y. Maeda, S. Sato, Y. Takano, F. Uhlik, Z. Slanina, Y. Lian, X. Lu, S. Nagase, M. M. Olmstead, A. L. Balch and T. Akasaka, *Chem. – Eur. J.*, 2016, **22**, 18115–18122.
11 J. Ding and S. Yang, *J. Am. Chem. Soc.*, 1996, **118**, 11254–11257.
12 H. Yang, H. Jin, X. Wang, Z. Liu, M. Yu, F. Zhao, B. Q. Mercado, M. M. Olmstead and A. L. Balch, *J. Am. Chem. Soc.*, 2012, **134**, 14127–14136.
13 H. Jin, H. Yang, M. Yu, Z. Liu, C. M. Beavers, M. M. Olmstead and A. L. Balch, *J. Am. Chem. Soc.*, 2012, **134**, 10933–10941.
14 B.-Y. Sun, T. Sugai, E. Nishibori, K. Iwata, M. Sakata, M. Takata and H. Shinohara, *Angew. Chem., Int. Ed.*, 2005, **44**, 4568–4571.
15 L. Bao, P. Yu, C. Pan, W. Shen and X. Lu, *Chem. Sci.*, 2019, **10**, 2153–2158.
16 M. Suzuki, X. Lu, S. Sato, H. Nikawa, N. Mizorogi, Z. Slanina, T. Tsuchiya, S. Nagase and T. Akasaka, *Inorg. Chem.*, 2012, **51**, 5270–5273.
17 X. Lu, Y. Lian, C. M. Beavers, N. Mizorogi, Z. Slanina, S. Nagase and T. Akasaka, *J. Am. Chem. Soc.*, 2011, **133**, 10772–10775.
18 W. Cai, R. Morales-Martinez, X. Zhang, D. Najera, E. L. Romero, A. Metta-Magana, A. Rodriguez-Fortea, S. Fortier, N. Chen, J. M. Poblet and L. Echegoyen, *Chem. Sci.*, 2017, **8**, 5282–5290.
19 Y. Wang, R. Morales-Martinez, X. Zhang, W. Yang, Y. Wang, A. Rodriguez-Fortea, J. M. Poblet, L. Feng, S. Wang and N. Chen, *J. Am. Chem. Soc.*, 2017, **139**, 5110–5116.
20 W. Cai, L. Abella, J. Zhuang, X. Zhang, L. Feng, Y. Wang, R. Morales-Martinez, R. Esper, M. Boero, A. Metta-Magana, A. Rodriguez-Fortea, J. M. Poblet, L. Echegoyen and N. Chen, *J. Am. Chem. Soc.*, 2018, **140**, 18039–18050.
21 P. W. Fowler and D. E. Manolopoulos, *An Atlas of Fullerenes*, Oxford University Press, Oxford, 1995.
22 T. Wei, F. Liu, S. Wang, X. Zhu, A. A. Popov and S. Yang, *Chem. – Eur. J.*, 2015, **21**, 5750–5759.
23 M. N. Chaur, X. Aparicio-Anglès, B. Q. Mercado, B. Elliott, A. Rodríguez-Fortea, A. Clotet, M. M. Olmstead, A. L. Balch, J. M. Poblet and L. Echegoyen, *J. Phys. Chem. C*, 2010, **114**, 13003–13009.
24 T. Zuo, C. M. Beavers, J. C. Duchamp, A. Campbell, H. C. Dorn, M. M. Olmstead and A. L. Balch, *J. Am. Chem. Soc.*, 2007, **129**, 2035–2043.
25 W. Q. Shen, L. P. Bao, S. F. Hu, X. J. Gao, Y. P. Xie, X. F. Gao, W. H. Huang and X. Lu, *Chem. – Eur. J.*, 2018, **24**, 16692–16698.
26 C. H. Chen, K. B. Ghiassi, M. R. Ceron, M. A. Guerrero-Ayala, L. Echegoyen, M. M. Olmstead and A. L. Balch, *J. Am. Chem. Soc.*, 2015, **137**, 10116–10119.
27 W. Shen, L. Bao, Y. Wu, C. Pan, S. Zhao, H. Fang, Y. Xie, P. Jin, P. Peng, F. F. Li and X. Lu, *J. Am. Chem. Soc.*, 2017, **139**, 9979–9984.
28 P. Jin, C. Liu, Y. Li, L. Li and Y. Zhao, *Int. J. Quantum Chem.*, 2018, **118**, e25501.
29 A. A. Popov, S. Yang and L. Dunsch, *Chem. Rev.*, 2013, **113**, 5989–6113.
30 T. Okazaki, Y. Lian, Z. Gu, K. Suenaga and S. Hisanori, *Chem. Phys. Lett.*, 2000, **320**, 435–440.
31 M. N. Chaur, F. Melin, B. Elliott, A. Kumbhar, A. J. Athans and L. Echegoyen, *Chem. – Eur. J.*, 2008, **14**, 4594–4599.
32 B. G. Burke, J. Chan, K. A. Williams, J. Ge, C. Shu, W. Fu, H. C. Dorn, J. G. Kushmerick, A. A. Puretzky and D. B. Geohegan, *Phys. Rev. B: Condens. Matter Mater. Phys.*, 2010, **81**, 115423.
33 J. Liu, Z. Shi and Z. Gu, *Chem. – Asian J.*, 2009, **4**, 1703–1711.

